

Structure–activity relationship study of copper(II) complexes with 2-oxo-1,2-dihydroquinoline-3-carbaldehyde (4'-methylbenzoyl) hydrazone: synthesis, structures, DNA and protein interaction studies, antioxidative and cytotoxic activity

Duraisamy Senthil Raja · Nattamai S. P. Bhuvanesh · Karuppanan Natarajan

Received: 28 April 2011 / Accepted: 3 September 2011 / Published online: 20 September 2011
© SBIC 2011

Abstract Novel 2-oxo-1,2-dihydroquinoline-3-carbaldehyde (4'-methylbenzoyl) hydrazone (H_2L) (**1**) and its two copper(II) complexes have been synthesized. Single-crystal X-ray diffraction studies revealed that the structure of the new copper(II) chloride complex, $[Cu(H_2L)Cl_2] \cdot 2H_2O$ (**2**), is square pyramidal and that of the copper(II) nitrate complex, $[Cu(HL)NO_3] \cdot DMF$ (**3**), is square planar. In **2**, the copper atom is coordinated by the ligand with ONO donor atoms, one chloride ion in the apical position, and the other chloride in the basal plane. In **3**, the ligand coordinates as a uninegative tridentate ONO^- species and with one nitrate ion in the basal plane. DNA binding experiments indicated that the ligand and copper(II) complexes can interact with DNA through intercalation. Bovine serum albumin binding studies revealed that the compounds strongly quench the intrinsic fluorescence of bovine serum albumin through a static quenching process. Antioxidative activity tests showed that **1** and its copper(II) complexes have significant radical scavenging activity against free radicals. Cytotoxic activities of the ligand and copper(II) complexes showed that the two copper(II) complexes exhibited more effective cytotoxic activity against HeLa and HEp-2 cells than the corresponding ligand. The entire biological activity results showed that the activity order was **1** < **2** < **3**.

Keywords Copper(II) complexes · DNA binding · Protein binding · Antioxidant · Cytotoxicity

Introduction

Metal complexes exert their anticancer effects through binding to DNA, thereby changing the replication of DNA and inhibiting the growth of the tumor cells, which is the basis for designing new and more efficient antitumor drugs [1, 2]. So, the design of small complexes that bind and react at specific sequences of DNA has become quite essential, and understanding the DNA binding properties of transition metal complexes is important because of their potential uses, such as drugs, regulators of gene expression, and tools for molecular biology [3–6]. Since the discovery of cisplatin, the synthesis of platinum complexes and their applications as antineoplastic agents have gained a lot of attention, whereas the inspiring clinical efficacy of cisplatin and related platinum-based drugs, as anticancer agents that bind covalently to DNA, is restricted by significant side effects such as nephrotoxicity, emetogenesis, neurotoxicity, and the emergence of drug resistance [7–10]. As a result, it is essential to design metal complexes of that are less toxic, target-specific, and preferably with noncovalent binding to DNA. To develop new anticancer drugs which specifically target DNA, it is necessary to understand the different noncovalent binding modes of metal complexes with DNA. Noncovalent binding modes are mainly classified as intercalation, groove binding, and electrostatic binding. Intercalation is one of the most important DNA binding modes because it invariably leads to cellular degradation. The planarity, coordination geometry, and type of donor atom present in ligands play key roles in determining the intercalating ability of complexes

D. Senthil Raja · K. Natarajan (✉)
Department of Chemistry,
Bharathiar University,
Coimbatore 641046, Tamil Nadu, India
e-mail: k_natraj6@yahoo.com

N. S. P. Bhuvanesh
Department of Chemistry,
Texas A&M University,
College Station, TX 77842, USA

with DNA [11–14]. The metal ion type and its valence, which are responsible for the geometry of the complexes, also influence the intercalating ability of metal complexes [15, 16]. In this regard, copper(II) complexes having square-planar and square-pyramidal geometry showed a remarkable intercalative binding affinity for DNA [17–20]. Moreover, the selective permeability of cancer cell membranes to copper complexes and their compact regulations of the intracellular concentration have encouraged the synthesis of copper-based drugs as potential anticancer agents that are projected to have less severe side effects [21]. On the other hand, many drugs, including anticoagulants, tranquilizers, anti-inflammatory drugs, and general anesthetics, are transported in the blood by combining with albumin [22]. Therefore, it is also worthwhile to study the interaction behaviors of the complexes with bovine serum albumin (BSA) before we move on to studying their radical scavenging and anticancer properties.

Quinolines are a broadly distributed class of compounds in nature with potentially advantageous effects in the field of medicine. Some derivatives of quinoline and 2-oxoquinoline have been shown to have biological activities such as antioxidation, antiproliferation, and anti-inflammation [23–27]. Furthermore, a great many hydrazones and their copper(II) complexes have also provoked immense interest in their diverse spectra of biological and pharmaceutical activities, such as anticancer, antitumor, and antioxidative activities [28–31]. In this regard, we have recently reported copper(II) complexes derived from 2-oxo-1,2-dihydroquinoline-3-carbaldehyde *N*-substituted thiosemicarbazones and their structure–activity relationship for biological properties such as protein binding and antioxidative and cytotoxic activity [32]. However, the structural and biological behaviors of hydrazone transition metal complexes derived from 2-oxo-1,2-dihydroquinoline-3-carbaldehyde have not been explored well. This aroused our interest in the synthesis of a new ligand, 2-oxo-1,2-dihydroquinoline-3-carbaldehyde (4'-methylbenzoyl) hydrazone (H_2L) (**1**), and its copper(II) complexes with a view towards evaluating the interaction behaviors of these compounds with DNA and BSA, and to explore their antioxidative and cytotoxic abilities.

Materials and methods

All chemicals were reagent grade and used without purification. 2-Oxo-1,2-dihydroquinoline-3-carbaldehyde was prepared according to the literature procedure [33]. Doubly distilled water was used to prepare buffers. Ethidium bromide (EB), BSA, and calf-thymus DNA (CT-DNA) were purchased from Sigma-Aldrich and used as received. Elemental analyses (C, H, N) were performed with a Vario EL

III Elementar analyzer. IR spectra (4,000–400 cm^{-1}) obtained with KBr disks were recorded with a Nicolet Avatar Fourier transform IR spectrophotometer. 1H NMR spectra were recorded with Bruker AMX 500 instrument at 500 MHz using tetramethylsilane as an internal standard. Melting points were determined with a Lab India instrument. Electronic absorption spectra were recorded using a JASCO V-630 spectrophotometer. Emission spectra were measured with a JASCO FP 6600 spectrofluorometer. Mass spectra were obtained with a VG ZAB-HS fast-atom bombardment (FAB) instrument. EPR spectra were recorded with a Bruker spectrometer operating at the X-band and using 100-kHz magnetic field modulation.

Solid-state magnetic susceptibility measurements were conducted at room temperature using a Faraday balance calibrated using mercury(II) tetrathiocyanatocobalt(II) as a calibrant. Molar conductivity was measured with a Systronic conductivity bridge with a dip-type cell, using a 5×10^{-3} M solution of complexes in 10% aqueous dimethyl sulfoxide (DMSO).

Synthesis of **1**

4-Methylbenzohydrazide (1.50 g, 0.01 mol) dissolved in warm methanol (50 mL) was added to a methanol solution (50 mL) containing 2-oxo-1,2-dihydroquinoline-3-carbaldehyde (1.73 g, 0.01 mol). The mixture was refluxed for 1 h, during which a light-yellow precipitate was formed. The reaction mixture was then cooled to room temperature and the solid compound (**1**) was filtered off. It was then washed with methanol and dried under a vacuum. Yield 91%. Melting point: 315–317 °C. Elemental analysis: found (calculated) (%) for $C_{18}H_{15}N_3O_2$: C, 70.73 (70.81); H, 4.99 (4.95); N, 13.72 (13.76). FAB mass spectrometry (MS): $m/z = 306$ (M + H). UV: λ_{max} (nm): 327, 377. IR: ν_{max} (cm^{-1}): $\nu_{C=O}$: 1,657, $\nu_{C=N}$: 1,558, ν_{N-H} : 3,280. 1H -NMR (DMSO- d_6 , 500 MHz, s, singlet; d, doublet; t, triplet; m, multiplet): δ 11.96 (s, 1H, N(3)H); 11.87 (s, 1H, N(2)H); 8.71 (s, 1H, C(1)H); 8.46 (s, 1H, C(6)H); 7.84–7.86 (d, 2H, C(7,10)H); 7.51–7.55 (t, 1H, C(9)H); 7.32–7.40 (m, 4H, C(13,14,16,17)H); 7.19–7.23 (t, 1H, C(8)H); 2.38 (s, 3H, C(18)H).

Synthesis of $[Cu(H_2L)Cl_2] \cdot 2H_2O$

A warm dimethylformamide (DMF) solution (10 mL) containing **1** (153 mg, 0.5 mmol) was added to a methanolic solution (20 mL) of $CuCl_2 \cdot 2H_2O$ (85 mg, 0.5 mmol). The resulting greenish solution was refluxed for 30 min. Green single crystals of $[Cu(H_2L)Cl_2] \cdot 2H_2O$ (**2**) suitable for X-ray studies were obtained on slow evaporation. They were filtered off, washed with cold methanol, and dried under vacuum. Yield: 85%. Melting point: 328–331 °C.

Elemental analysis: found (calculated) (%) for $C_{18}H_{19}Cl_2CuN_3O_4$: C, 45.18 (45.44); H, 4.11 (4.02); N, 8.71 (8.83). UV: λ_{\max} (nm): 350, 380. IR: ν_{\max} (cm^{-1}): $\nu_{C=O}$: 1,653, $\nu_{C=N}$: 1,547. μ_{eff} (27 °C): 1.71 μ_B . EPR (at room temperature): $g = 2.16$ (solid), 2.14 (10% aqueous DMSO). Molar conductivity: Λ_M ($S \text{ mol}^{-1} \text{ cm}^2$): 0.41.

Synthesis of $[Cu(HL)NO_3] \cdot DMF$

It was prepared by the same procedure as described for **2** using H_2L (153 mg (0.5 mmol) and $Cu(NO_3)_2 \cdot 3H_2O$ (121 mg, 0.5 mmol). Green single crystals of $[Cu(HL)NO_3] \cdot DMF$ (**3**) were obtained. Yield 87%. Melting point: 325–327 °C. Elemental analysis: found (calculated) (%) for $C_{21}H_{21}CuN_5O_6$: C, 50.07 (50.15); H, 4.22 (4.21); N, 13.87 (13.92). UV: λ_{\max} (nm): 263, 368, 403, 423. IR: ν_{\max} (cm^{-1}): $\nu_{C=O}$: 1,638, $\nu_{C=N}$: 1,549. μ_{eff} (27 °C): 1.73 μ_B . EPR (at room temperature): $g = 2.13$ (solid), 2.17 (10% aqueous DMSO). Molar conductivity: Λ_M ($S \text{ mol}^{-1} \text{ cm}^2$): 0.38.

Crystallography

Single-crystal X-ray diffraction data of **2** and **3** were collected with a Bruker three-circle platform diffractometer equipped with a SMART 1000 CCD detector. Integrated intensity information for each reflection was obtained by reduction of the data frames with the program APEX2 [34]. All non-hydrogen atoms were refined with anisotropic thermal parameters. The hydrogen atoms bound to carbon were placed in idealized positions and refined using a riding model. Hydrogen atoms attached to nitrogen and oxygen were located from the Fourier difference maps and were set riding on the respective parent atom. The structures were refined (weighted least-squares refinement on F^2) to convergence [35]. Relevant data concerning data collection and details of structure refinement are summarized in Table 1. Crystallographic data (without structure factors) for the structures reported in this article have been deposited with the Cambridge Crystallographic Data Centre (CCDC) as supplementary publication numbers

Table 1 Experimental data for crystallographic analyses

| | 2 | 3 |
|--|--|--|
| Empirical formula | $C_{18}H_{19}Cl_2CuN_3O_4$ | $C_{21}H_{21}CuN_5O_6$ |
| Formula weight | 475.80 | 502.97 |
| Temperature (K) | 110(2) | 110(2) |
| Wavelength (Å) | 0.71073 | 0.71073 |
| Crystal system | Monoclinic | Triclinic |
| Space group | $P2(1)/c$ | $P-1$ |
| Cell dimensions | | |
| a (Å) | 7.643(6) | 7.672(3) |
| b (Å) | 9.759(8) | 10.865(4) |
| c (Å) | 25.60(2) | 12.670(5) |
| α (°) | 90 | 80.502(6) |
| β (°) | 94.115(10) | 83.745(6) |
| γ (°) | 90 | 84.813(6) |
| Volume (Å ³) | 1,905(3) | 1,032.6(7) |
| Z | 4 | 2 |
| Density (Mg/m^3) | 1.659 | 1.618 |
| $F(000)$ | 972 | 518 |
| Crystal size (mm^3) | $0.50 \times 0.50 \times 0.08$ | $0.71 \times 0.27 \times 0.17$ |
| Index ranges | $-9 \leq h \leq 9, -11 \leq k \leq 12, -32 \leq l \leq 31$ | $-9 \leq h \leq 9, -14 \leq k \leq 14, -16 \leq l \leq 16$ |
| Reflections collected | 15,101 | 11,779 |
| Independent reflections | 4,292 [$R(\text{int}) = 0.0892$] | 4,659 [$R(\text{int}) = 0.0305$] |
| Absorption correction | Semiempirical from equivalents | Semiempirical from equivalents |
| Maximum and minimum transmission | 0.8923 and 0.5292 | 0.8338 and 0.5064 |
| Refinement method | Full-matrix least squares on F^2 | Full-matrix least squares on F^2 |
| Data/restraints/parameters | 4,292/0/253 | 4,659/0/300 |
| Goodness of fit on F^2 | 1.069 | 1.047 |
| Final R indices [$I > 2\sigma(I)$] | $R_1 = 0.0516, wR_2 = 0.1271$ | $R_1 = 0.0265, wR_2 = 0.0713$ |
| R indices (all data) | $R_1 = 0.0601, wR_2 = 0.1311$ | $R_1 = 0.0298, wR_2 = 0.0730$ |

CCDC-783730 and CCDC-787359 for **2** and **3**, respectively. Copies of the data can be obtained free of charge from the CCDC (12 Union Road, Cambridge CB2 1EZ, UK; Tel: +44-1223-336408; Fax: +44-1223-336003; e-mail: deposit@ccdc.cam.ac.uk; Web site: <http://www.ccdc.cam.ac.uk>).

DNA interaction experiments

All the experiments involving the binding of compounds **1**, **2**, and **3** with CT-DNA were conducted in a doubly distilled water buffer with 5 mM tris(hydroxymethyl)aminomethane (Tris) and 50 mM sodium chloride and adjusted to pH 7.2 with hydrochloric acid. A solution of CT-DNA in the buffer gave a UV absorbance ratio of about 1.9 at 260 and 280 nm, indicating that the DNA was sufficiently free of protein. The DNA concentration per nucleotide was determined by absorption spectroscopy using the molar extinction coefficient value of $6,600 \text{ dm}^3 \text{ mol}^{-1} \text{ cm}^{-1}$ at 260 nm. The compounds were dissolved in a mixed solvent of 5% DMSO and 95% Tris-HCl buffer. Absorption titration experiments were performed with fixed concentrations of the compounds (25 μM) while gradually increasing the concentration of DNA (2.5–25 μM). While measuring the absorption spectra, we added an equal amount of DNA to both the compound solution and the reference solution to eliminate the absorbance of DNA itself. The same experimental procedure was also followed for emission studies. All the compounds were excited at 375 nm and their corresponding emission spectra was monitored in the range from 400 to 540 nm.

EB-DNA experiments were conducted by adding the solution of the compounds to the Tris-HCl buffer of EB-DNA. The change of fluorescence intensity was recorded. The excitation and the emission wavelengths were 515 and 602 nm, respectively. According to the classical Stern-Volmer equation,

$$I_0/I = K_q[Q] + 1,$$

where I_0 is the emission intensity in the absence of the quencher, I is the emission intensity in the presence of the quencher, K_q is the quenching constant, and $[Q]$ is the quencher concentration. The K_q value is obtained as a slope from the plot of I_0/I versus $[Q]$.

Protein binding studies

An excitation wavelength of 280 nm was chosen since it provides excitation of both tryptophan and tyrosine residues, and the emission of both residues at 346 nm was monitored for the protein binding studies. The excitation and emission slit widths and scan rates were maintained constant for all the experiments. Samples were carefully degassed using pure nitrogen gas for 15 min. Quartz cells (4 cm \times 1 cm \times 1 cm) with high-vacuum Teflon stopcocks were used for

degassing. Stock solution of BSA was prepared in 50 mM phosphate buffer (pH 7.2) and stored in the dark at 4 $^\circ\text{C}$ for further use. Concentrated stock solution of compounds were prepared by dissolving the compounds in DMSO-phosphate buffer (1:50) and were diluted suitably with phosphate buffer to required concentrations for all the experiments. Titrations were done manually by using a micropipette for the addition of compounds. If it is assumed that the binding of compounds to BSA occurs at equilibrium, the equilibrium binding constant can be analyzed according to the Scatchard equation:

$$\log [(I_0 - I)/I] = \log K_{\text{bin}} + n \log [Q],$$

where K_{bin} is the binding constant of the compound with BSA and n is the number of binding sites. The value of K_{bin} can be determined from the slope of the plot of $\log [(I_0 - I)/I]$ versus $\log [Q]$. For synchronous fluorescence spectra, the same concentrations of BSA and compounds were used and the spectra were measured at two different $\Delta\lambda$ (difference between the excitation and emission wavelengths of BSA) values, such as 15 and 60 nm.

Antioxidant assays

The 2,2'-diphenyl-1-picrylhydrazyl (DPPH) radical scavenging activity of the compounds was measured according to the method of Blais [36]. The DPPH radical is a stable free radical having λ_{max} at 517 nm. A fixed concentration of the experimental compound was added to solution of DPPH in methanol (125 μM , 2 mL) and the final volume was made up to 4 mL with doubly distilled water. The solution was incubated at 37 $^\circ\text{C}$ for 30 min in the dark. The decrease in absorbance of DPPH was measured at 517 nm.

The hydroxyl (OH) radical scavenging activities of the complexes have been investigated using the Nash method [37]. In vitro hydroxyl radicals were generated by an Fe^{3+} -ascorbic acid system. The detection of hydroxyl radicals was performed by measuring the amount of formaldehyde formed from the oxidation reaction with DMSO. The formaldehyde produced was detected spectrophotometrically at 412 nm. A mixture of 1.0 mL iron-EDTA solution (0.13% ferrous ammonium sulfate and 0.26% EDTA), 0.5 mL EDTA solution (0.018%), and 1.0 mL DMSO (0.85% v/v DMSO in 0.1 M phosphate buffer, pH 7.4) were sequentially added to the test tubes. The reaction was initiated by adding 0.5 mL ascorbic acid (0.22%) and the mixture was incubated at 80–90 $^\circ\text{C}$ for 15 min in a water bath. After incubation, the reaction was terminated by the addition of 1.0 mL ice-cold trichloroacetic acid (17.5% w/v). Subsequently, 3.0 mL Nash reagent was added to each tube and the tubes were left at room temperature for 15 min. The intensity of the color formed was measured spectrophotometrically at 412 nm against a reagent blank.

Assay of nitric oxide (NO) scavenging activity is based on the method in [38], where sodium nitroprusside in aqueous solution at physiological pH spontaneously generates nitric oxide, which interacts with oxygen to produce nitrite ions that can be estimated using Griess reagent. Scavengers of nitric oxide compete with oxygen, leading to reduced production of nitrite ions. For the experiment, sodium nitroprusside (10 mM) in phosphate-buffered saline was mixed with a fixed concentration of the compound and the mixture was incubated at room temperature for 150 min. After the incubation period, 0.5 mL of Griess reagent containing 1% sulfanilamide, 2% H₃PO₄, and 0.1% *N*-(1-naphthyl) ethylenediamine dihydrochloride was added. The absorbance of the chromophore formed was measured at 546 nm.

The superoxide (O₂^{•-}) radical scavenging assay was based on the capacity of the compounds to inhibit formazan formation by scavenging the superoxide radicals generated in a riboflavin–light–nitroblue tetrazolium system [39]. Each 3 mL reaction mixture contained 50 mM sodium phosphate buffer (pH 7.6), 20 μg riboflavin, 12 mM EDTA, 0.1 mg nitroblue tetrazolium, and 1 mL complex solution (20–100 μg/mL). The reaction was started by illuminating the reaction mixture with different concentrations of the complex for 90 s. Immediately after illumination, the absorbance was measured at 590 nm. The entire reaction assembly was enclosed in a box lined with aluminum foil. Identical tubes with reaction mixture kept in the dark served as blanks.

For the four assays described above, all the tests were run in triplicate and various concentrations of the compounds were used to fix a concentration at which the compounds showed around 50% of activity. In addition, the percentage of activity was calculated using the following formula: percentage of activity = [(A₀ - A_C)/A₀] × 100 (A₀ and A_C are the absorbance in the absence and presence of the compound tested, respectively). The 50% of activity (IC₅₀) can be calculated using the percentage of activity results.

In vitro anticancer activity evaluation by 3-(4,5-dimethylthiazol-2-yl)-2,5-diphenyltetrazolium bromide assays

Cytotoxicity studies of the compounds and cisplatin were conducted on human cervical cancer cells (HeLa), human laryngeal epithelial carcinoma cells (HEp-2), and NIH 3T3 mouse embryonic fibroblasts, which were obtained from the National Centre for Cell Science, Pune, India. Cell viability was investigated using the 3-(4,5-dimethylthiazol-2-yl)-2,5-diphenyltetrazolium bromide (MTT) assay method [40]. The HeLa and HEp-2 cells were grown in Eagle's minimum essential medium containing 10% fetal

bovine serum (FBS). NIH 3T3 fibroblasts were grown in Dulbecco's modified Eagle's medium containing with 10% FBS. For screening experiments, the cells were seeded into 96-well plates in 100 μL of the respective medium containing 10% FBS, at a plating density of 10,000 cells per well, and were incubated at 37 °C, 5% CO₂, 95% air, and 100% relative humidity for 24 h prior to addition of the compounds. The compounds were dissolved in DMSO and diluted in the respective medium containing 1% FBS. After 24 h, the medium was replaced with the respective medium with 1% FBS containing the compounds at various concentrations and the mixture was incubated at 37 °C, 5% CO₂, 95% air, and 100% relative humidity for 48 h. Triplicate analyses were performed and the medium without the compounds served as a control. After 48 h, 10 μL MTT (5 mg/mL) in phosphate-buffered saline was added to each well and the wells were incubated at 37 °C for 4 h. The medium with MTT was then flicked off and the formazan crystals that had formed were dissolved in 100 μL DMSO. Then the absorbance at 570 nm was measured using a microplate reader. The percentage of cell inhibition was determined using the following formula: percentage of inhibition = [mean optical density of untreated cells (control)/mean optical density of treated cells (control)] × 100. A graph of the percentage of cell inhibition versus concentration was plotted and from this the IC₅₀ value was calculated.

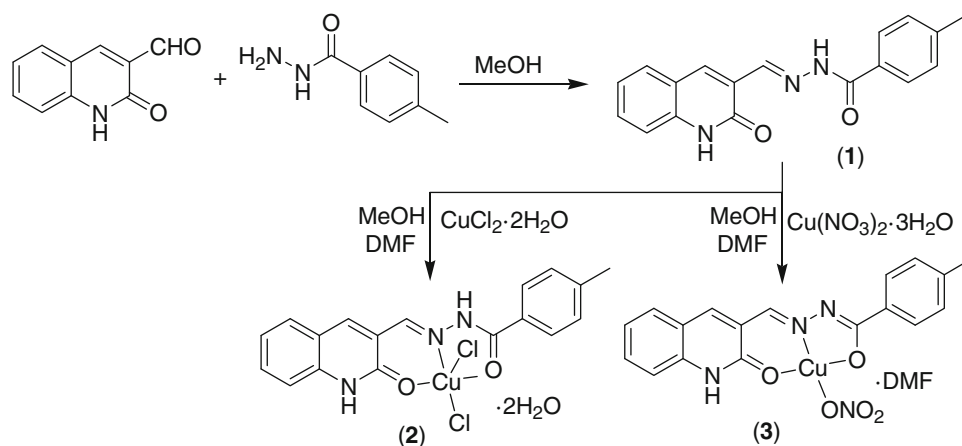
Results and discussion

Synthesis and characterization

The synthetic routes for the ligand (**1**) and its copper(II) complexes are shown in Scheme 1. The ligand was prepared by the condensation reaction of 2-oxo-1,2-dihydroquinoline-3-carbaldehyde with 4-methylbenzohydrazide in methanol medium. It was characterized by elemental analysis, IR spectroscopy, ¹H NMR spectroscopy, and FAB-MS. The FAB mass spectra of the ligand showed a peak at *m/z* = 306 for (M + H) and the measured molecular weight was consistent with the expected value. The assignments for the IR and ¹H NMR spectra are given in "Materials and methods." The copper(II) complexes were prepared by the direct reaction of the ligand with copper(II) salts in DMF and methanol medium.

The single crystals of new copper(II) complexes were isolated by slow evaporation of the reaction mixture over a period of 2–3 months. The IR peak shift of ν_{C=O} and ν_{C=N} of the ligand in the complex give an idea of its coordination to copper. The experimental μ_{eff} values of 1.71 and 1.73 for the two complexes confirmed the +2 oxidation state of copper in the complexes. All the compounds are soluble in

Scheme 1 The synthetic route for the ligand and its copper(II) complexes. *DMF* dimethylformamide



methanol, ethanol, DMF, and DMSO and are stable in air. X-band EPR spectra of the complexes at room temperature showed a single isotropic resonance with g values of 2.16 and 2.14 for **2** and 2.13 and 2.17 for **3** for the powdered and 10% aqueous DMSO solution of the complexes, respectively, indicating that the two copper(II) complexes retained their solid-state structure in aqueous solution. Moreover, the molar conductivities of copper(II) complexes in 10% aqueous DMSO were measured to find out the labile nature of the coordinated chloride and nitrate in aqueous solution. The conductance values measured (Λ_M of 0.41 and 0.38 $\text{S mol}^{-1} \text{cm}^2$ for **2** and **3**, respectively) were too low to account for any dissociation; hence the two copper(II) complexes were considered to be nonelectrolytes and were quite stable in aqueous solution. The structures of the new copper(II) complexes

were finally confirmed by single-crystal X-ray crystallographic studies.

X-ray structural characterization

The ORTEP view of the neutral complex $[\text{Cu}(\text{H}_2\text{L})\text{Cl}_2] \cdot 2\text{H}_2\text{O}$ (**2**) is given in Fig. 1. The ligand is coordinated as a neutral moiety in an ONO fashion and the other two coordination sites are filled by chloride ions completing a square-pyramidal geometry around the copper ion in complex **2**. The copper atom lies about 0.166 Å above the average basal plane towards the axial Cl2 atom in **2**.

The pyramid is fairly regular and the axial Cu–Cl bond length is longer than that of the basal one, which can be ascribed to Jahn–Teller distortion. The dihedral angle between the mean planes of the five-membered chelate ring

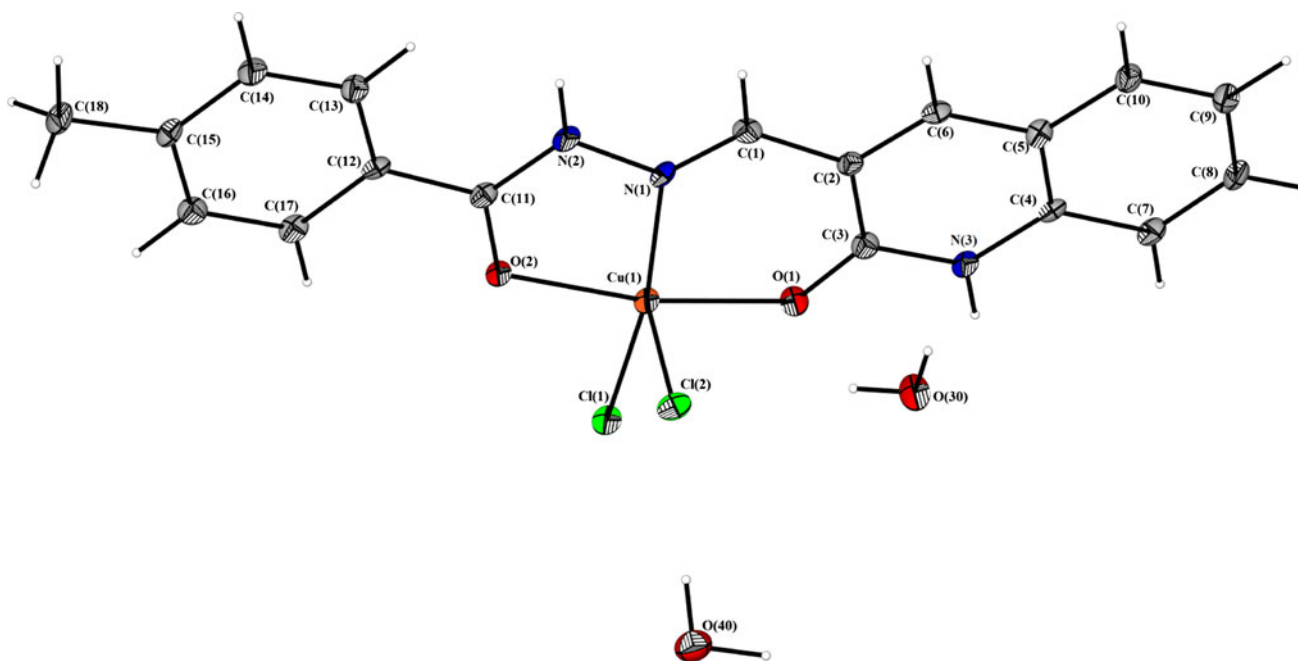


Fig. 1 ORTEP view of the molecular structure and atom-labeling scheme of **2**. Thermal ellipsoids are drawn at the 50% probability level

and the six-membered one is 4.49° for **2**. Since the hydrazone moieties have both hydrogen-bond donors and hydrogen-bond acceptors, the species provide the possibility of forming hydrogen bonds in the crystal. In fact, the crystal lattice of the complex showed a three-dimensional array in which each unit of the complex is hydrogen-bonded to the other involving N2 and N3 nitrogen atoms, the O30 and O40 oxygen atoms of water molecules, and the C11 and C12 chlorine atoms.

An ORTEP view of $[\text{Cu}(\text{HL})\text{NO}_3]\cdot\text{DMF}$ (**3**) is given in Fig. 2. Complex **3** contains a tetracoordinated copper(II) ion with one ONO tridentate uninegative ligand and one nitrate ion coordinated through oxygen with one DMF molecule in the lattice.

The N1–Cu–O2 bond angle [$81.67(6)^\circ$] is significantly smaller than that of other three [bond angles of N1–Cu–O1, O2–Cu–O3, and O1–Cu–O3 are $92.47(6)^\circ$, $95.00(5)^\circ$, and $92.15(5)^\circ$, respectively], indicating a slightly distorted square-planar geometry around the copper atom in the complex. Unlike in **2**, O2 is coordinated as a negative donor (enolate and not keto form) in **3**. This may be due to the strong electron-withdrawing nature of nitrate compared

with chloride. A very short distance (0.019 \AA) between the copper atom and the average basal plane and a small dihedral angle (3.72°) between the mean planes of the five-membered chelation ring and the six-membered one ensures that the planarity of the square should be appreciable. The molecular packing suggests that the stabilization of the lattice must have been due to several hydrogen bonds, mainly involving the N3 and O34 atoms. Selected bond distances and bond angles of **2** and **3** are given in Table 2 and agree well with those found in related copper complexes [41, 42].

DNA binding activity

Electronic absorption spectroscopy is one of the most useful techniques for DNA binding studies of small molecules. The absorption spectra of copper(II) complexes **2** and **3** and the ligand (**1**) in the absence and presence of CT-DNA are given in Fig. 3. In the presence of CT-DNA, the absorption bands of the ligand at 326 and 367 nm exhibited hypochromism of about 24 and 25% respectively. Square-pyramidal complex **2** exhibited hypochromism of

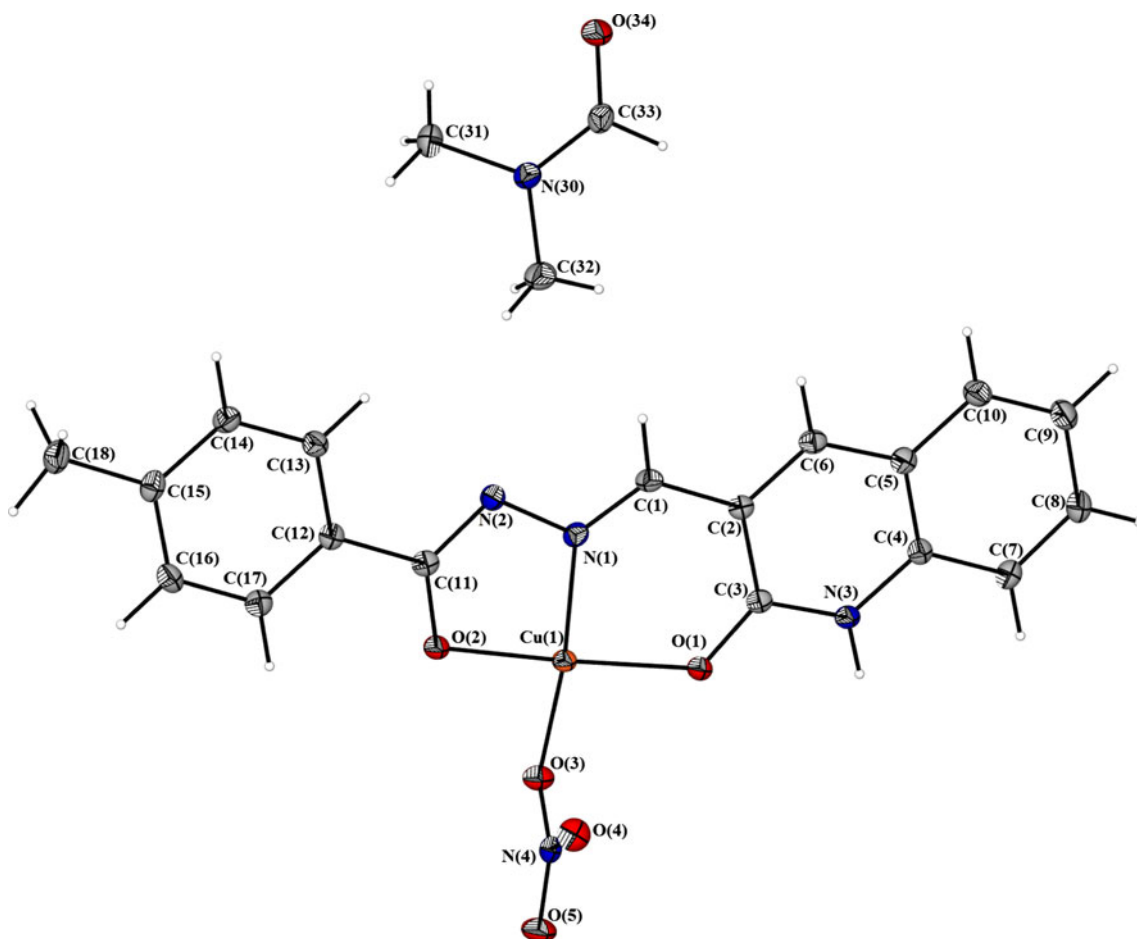


Fig. 2 ORTEP view of the molecular structure and atom-labeling scheme of **3**. Thermal ellipsoids are drawn at the 50% probability level

Table 2 Selected bond lengths (Å) and angles (°) for **2** and **3**

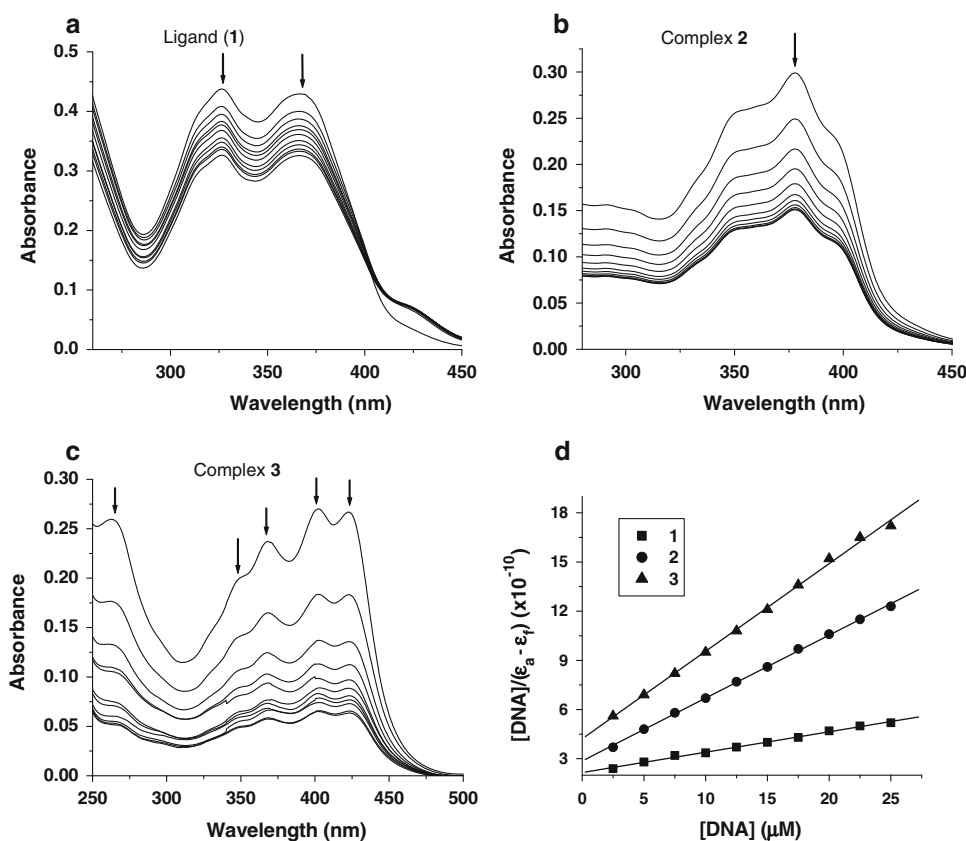
| | 2 | 3 |
|-------------------|------------|------------|
| Cu(1)–O(1) | 1.927(3) | 1.9474(12) |
| Cu(1)–O(2) | 1.950(2) | 1.9359(12) |
| Cu(1)–N(1) | 1.967(3) | 1.9243(14) |
| Cu(1)–Cl(1) | 2.2232(16) | |
| Cu(1)–Cl(2) | 2.733(2) | |
| Cu(1)–O(3) | | 1.9599(12) |
| C(11)–O(2) | 1.260(4) | 1.2946(18) |
| C(11)–N(2) | 1.337(4) | 1.326(2) |
| N(1)–N(2) | 1.380(4) | 1.3831(18) |
| O(1)–Cu(1)–O(2) | 169.93(10) | 170.01(5) |
| O(1)–Cu(1)–N(1) | 91.67(11) | 92.47(6) |
| O(2)–Cu(1)–N(1) | 80.89(11) | 81.67(6) |
| O(1)–Cu(1)–Cl(1) | 93.48(8) | |
| O(2)–Cu(1)–Cl(1) | 92.49(8) | |
| N(1)–Cu(1)–Cl(1) | 167.24(8) | |
| O(1)–Cu(1)–Cl(2) | 94.10(9) | |
| O(2)–Cu(1)–Cl(2) | 91.86(8) | |
| N(1)–Cu(1)–Cl(2) | 83.93(8) | |
| Cl(1)–Cu(1)–Cl(2) | 107.31(4) | |
| N(1)–Cu(1)–O(3) | | 169.45(5) |
| O(2)–Cu(1)–O(3) | | 95.00(5) |
| O(1)–Cu(1)–O(3) | | 92.15(5) |

about 49% at 378 nm. On the other hand, the square-planar complex (**3**) exhibited hypochromism of about 79, 81, and 80% at 368, 403, and 423 nm, respectively. To illustrate quantitatively the consequence, the absorption data were analyzed to evaluate the intrinsic binding constant (K_b), which can be determined from the following equation:

$$[\text{DNA}]/(\varepsilon_a - \varepsilon_f) = [\text{DNA}]/(\varepsilon_b - \varepsilon_f) + 1/K_b(\varepsilon_b - \varepsilon_f),$$

where [DNA] is the concentration of DNA in base pairs, and the apparent absorption coefficients ε_a , ε_f , and ε_b correspond to $A_{\text{obs}}/[\text{compound}]$, the extinction coefficient of the free compound, and the extinction coefficient of the compound when fully bound to DNA, respectively. From the plot of $[\text{DNA}]/(\varepsilon_a - \varepsilon_f)$ versus [DNA] (Fig. 3d), K_b is calculated from the ratio of the slope to the intercept. The calculated K_b values of $2.02(\pm 0.07) \times 10^5 \text{ M}^{-1}$, $4.59(\pm 0.17) \times 10^5 \text{ M}^{-1}$, and $9.08(\pm 0.27) \times 10^5 \text{ M}^{-1}$ for compounds **1**, **2**, and **3**, respectively, suggested an intimate association of the compounds with CT-DNA, and it is also likely that these compounds bind to the helix via intercalation [43]. After the compounds have intercalated themselves among the base pairs of DNA, the π^* orbital of the intercalated compounds can couple with π orbitals of the base pairs, thus decreasing the $\pi \rightarrow \pi^*$ transition energies. Therefore, these interactions resulted in the observed hypochromism [44]. Complexes **2** and **3** showed more

Fig. 3 Absorption spectra of compounds **1** (a), **2** (b), and **3** (c) (25 μM) in the presence of increasing amounts of calf-thymus DNA (CT-DNA) (0, 2.5, 5, 7.5, 10, 12.5, 15, 17.5, 20, 22.5, 25 μM). Arrows show the absorbance changes upon increasing DNA concentration. d Plots of $[\text{DNA}]/(\varepsilon_a - \varepsilon_f)$ versus [DNA] for the titration of compounds with CT-DNA



hypochromicity and higher K_b values than the ligand, indicating that the binding strength of the copper(II) complexes is much greater than that of the free ligand. From the electronic absorption studies, although it was found that the three compounds can bind to DNA by intercalation, the binding mode need to be proved through some more experiments. Hence, to start with we conducted emission experiments to investigate the interactions between the compounds studied and CT-DNA.

The enhancements in the emission intensity of the compounds with increasing CT-DNA concentrations are shown in Fig. 4. In the absence of DNA, compounds **1**, **2**, and **3** weakly luminescence in Tris buffer when excited at 375 nm. The intensity of the emission for compounds **1**, **2**, and **3** increases with the increase of DNA concentration. Upon the addition of CT-DNA, the emission intensities at 450 nm were increased by around 2 and 3 times for complexes **2** and **3**, respectively. But, the emission intensity of the ligand (**1**) at 442 nm increased only around 1.5 times. This phenomenon is related to the extent to which the compound penetrates into the hydrophobic environment inside the DNA, thereby avoiding the quenching effect of solvent water molecules. The binding of complexes **2** and **3** and free ligand to CT-DNA leads to a marked increase in the emission intensity, which also agrees with the increases observed for other intercalators [45]. These results show that the complexes bind more strongly than the free ligand. From the observed intensity enhancement of the two complexes in the presence of CT-DNA, it can be seen that **3** has more DNA binding ability than **2**. The higher binding affinity of the copper(II) complexes is attributed to the extension of the π system of the intercalated ligand due to the coordination to the copper(II) ion. Since the complexes have planar area greater than that of the free ligand, leading the complexes to penetrate more deeply into and stack more strongly with the base pairs of the DNA.

In the second investigation, emission quenching experiments were conducted.

EB is one of the most sensitive fluorescent probes which can bind to DNA through intercalation [46, 47]. Competitive binding to DNA of drugs with EB could provide rich information with regard to the DNA binding affinity. Figure 5 shows the emission spectra of the DNA–EB system with increasing amounts of **1**, **2**, and **3**.

The emission intensity of the DNA-EB system decreased, apparently as the concentration of complexes **2** and **3** and free ligand increased. This is because EB is expelled from the hydrophobic environment into the water solution [48]. Quenching data were analyzed according to the Stern–Volmer equation, which could be used to determine the fluorescence quenching mechanism. The quenching plots illustrate that the quenching of EB bound to CT-DNA by **2**, **3**, and the free ligand (**1**) is in good agreement with the linear Stern–Volmer equation, which also proves that they bind to DNA. In the Stern–Volmer plots (Fig. 5d) of I_0/I versus $[Q]$, the quenching constant (K_q) is given by the ratio of the slope to the intercept. Further, the value of the binding constant (K_{app}) for the compounds can be obtained by using the following equation:

$$K_{EB}[EB] = K_{app}[\text{compound}],$$

where the compound concentration is the value at a 50% reduction of the fluorescence intensity of EB, $K_{EB} = 1.0 \times 10^7 \text{ M}^{-1}$, and $[EB] = 0.25 \mu\text{M}$. The calculated K_q and K_{app} values are given in Table 3.

These data suggest that the interaction of the copper(II) complexes with CT-DNA is stronger than that of the free ligand, which is consistent with the above absorption and emission spectral observations. Since these changes indicate only one kind of quenching process, it may be concluded that **1**, **2**, and **3** bind to CT-DNA via the same mode.

Furthermore, such quenching constants and binding constants of the ligand and copper(II) complexes suggest

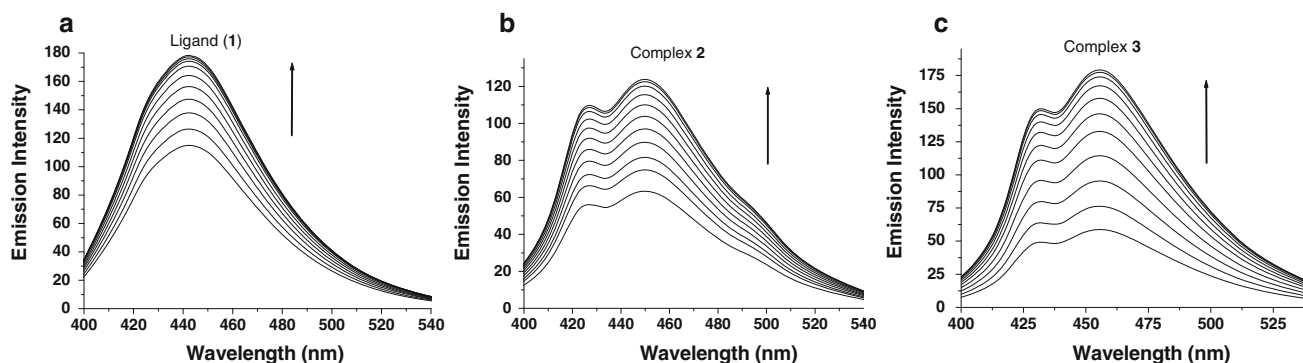


Fig. 4 Emission enhancement spectra of compounds **1** (a), **2** (b), and **3** (c) (25 μM) in the presence of increasing amounts of CT-DNA (0, 2.5, 5, 7.5, 10, 12.5, 15, 17.5, 20, 22.5, 25 μM) ($\lambda_{ex} = 375 \text{ nm}$,

$\lambda_{em} = 400\text{--}540 \text{ nm}$). Arrows show the emission intensity changes upon increasing DNA concentration

Fig. 5 Emission spectra of the DNA–ethidium bromide (EB) system (25 μM DNA and 0.25 μM EB), $\lambda_{\text{ex}} = 510$ nm, $\lambda_{\text{em}} = 530\text{--}700$ nm, in the presence of 0, 1, 2, 3, 4, and 5 μM **1** (a), **2** (b), and **3** (c). Arrows show the emission intensity changes upon increasing concentration of the compounds. **d** Stern–Volmer plots of the fluorescence titration of **1**, **2**, and **3**

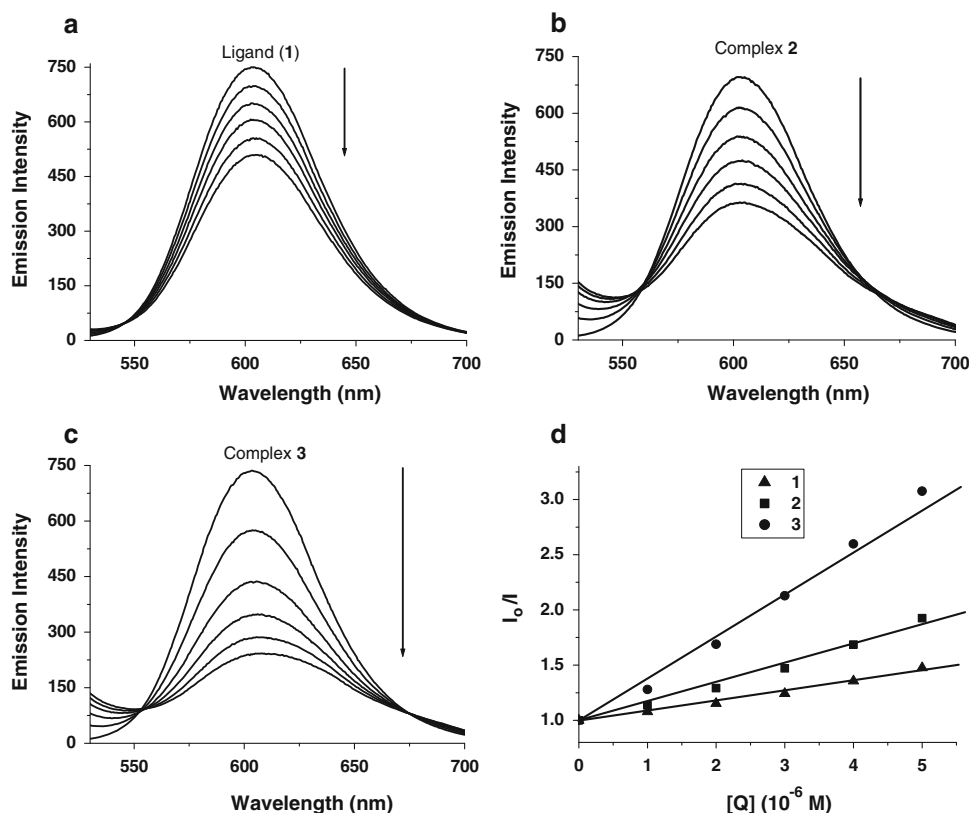


Table 3 Quenching constant (K_q) and binding constant (K_{app}) for the interactions of compounds with DNA

| Compound | K_q (M^{-1}) | K_{app} (M^{-1}) |
|----------|-------------------------------|--------------------------------------|
| 1 | $8.93 (\pm 0.25) \times 10^4$ | $2.23 (\pm 0.15) \times 10^5$ |
| 2 | $1.73 (\pm 0.17) \times 10^5$ | $4.33 (\pm 0.10) \times 10^5$ |
| 3 | $3.97 (\pm 0.12) \times 10^5$ | $9.93 (\pm 0.18) \times 10^5$ |

that the interaction of all the compounds with DNA should be by intercalation [49]. On the basis of all the spectroscopic studies, we come to the conclusion that the copper(II) complexes and the free ligand can bind to CT-DNA in an intercalative mode and that the copper(II) complexes bind to CT-DNA more strongly than the free ligand. Among the two copper(II) complexes, the square-planar complex (**3**) has greater binding ability than the square-pyramidal complex (**2**) because the square-planar geometry allows it to more easily intercalate itself among the base pairs of DNA in comparison with the square-pyramidal geometry.

BSA binding activity

Serum albumin is the most abundant protein in plasma. Therefore, it is important to consider the interactions of bioactive compounds with plasma proteins, particularly with serum albumin. Binding to these proteins may lead to

loss or enhancement of the biological properties of the original compounds, or may provide paths for their transportation. BSA is the most extensively studied serum albumin, owing to its structural homology with human serum albumin. The interaction of BSA with our compounds was studied by fluorescence measurements at room temperature. A solution of BSA (1 μM) was titrated with various concentrations of the complex (0–5 μM).

Fluorescence spectra were recorded in the range from 290 to 450 nm upon excitation at 280 nm. The effect of the compounds on the fluorescence spectrum of BSA is shown in Fig. 6. Addition of the compounds to a solution of BSA resulted in a significant decrease of the fluorescence intensity of BSA at 346 nm, up to 45.7, 54.5, and 59.1% of the initial fluorescence intensity of BSA, accompanied by a small blueshift of 3, 5, and 6 nm for **1**, **2**, and **3**, respectively. The observed blueshift is mainly due to the fact that the active site in the protein is buried in a hydrophobic environment. This result suggested a definite interaction of all three compounds with the BSA protein. The fluorescence quenching mechanisms are usually classified as either static or dynamic quenching. A simple method to explore the type of quenching is UV–vis absorption spectroscopy. UV–vis spectra of BSA in the absence and presence of the compounds (Fig. 7) show that the absorption intensity of BSA was enhanced as the compounds were added, and there was a small blueshift.

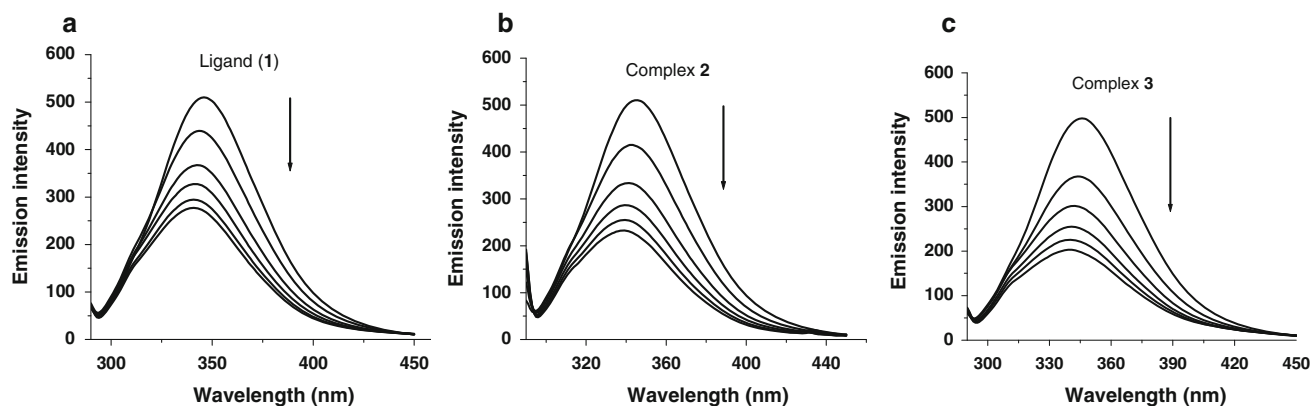


Fig. 6 The emission spectrum of bovine serum albumin (BSA) ($1 \mu\text{M}$; $\lambda_{\text{ex}} = 280 \text{ nm}$, $\lambda_{\text{em}} = 346 \text{ nm}$) in the presence of increasing amounts of compounds **1** (a), **2** (b), and **3** (c) (0, 1, 2, 3, 4, and 5 μM).

Arrows show the fluorescence quenching upon increasing the concentration of the compounds

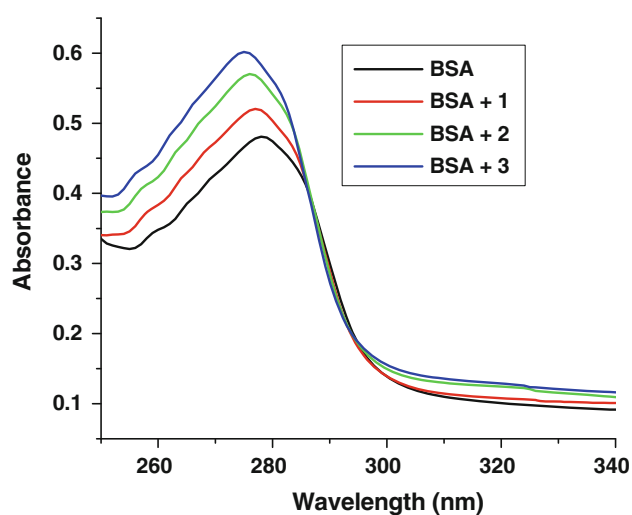


Fig. 7 Absorption spectra of BSA ($10 \mu\text{M}$), and with compounds **1**, **2**, and **3** ($5 \mu\text{M}$)

As is well known, dynamic quenching only affects the excited state of fluorophores but does not change the absorption spectrum. However, the formation of a

nonfluorescent ground-state complex induces a change in the absorption spectrum of fluorophores, suggesting the possible quenching mechanism of BSA by the compounds is a static quenching process [50]. To elucidate the quenching mechanism further, fluorescence quenching data were analyzed with the Stern–Volmer equation and the Scatchard equation. The quenching constant (K_q) can be calculated using the plot of I_0/I versus $[Q]$ (Fig. 8a).

From the plot of $\log(I_0 - I)/I$ versus $\log [Q]$ (Fig. 8b), the number of binding sites (n) and the binding constant (K_{bin}) were obtained. The calculated K_q , K_{bin} , and n values are given in Table 4. The calculated value of n is around 1 for all the compounds, indicating the existence of just a single binding site in BSA for all the compounds. The values of K_q and K_{bin} for **1**, **2**, and **3** suggested that the complexes interact with BSA more strongly than does the ligand. In particular, the square-planar complex (**3**) has better interaction with BSA than the square-pyramidal complex (**2**). The binding constants are very comparable to the binding constants of many biologically valuable drugs found in the literature [51–53]. Moreover, the stronger binding ability of the compounds with BSA clearly

Fig. 8 a Stern–Volmer plots of the fluorescence titration of **1**, **2**, and **3** with BSA. b Scatchard plots of the fluorescence titration of **1**, **2**, and **3** with BSA

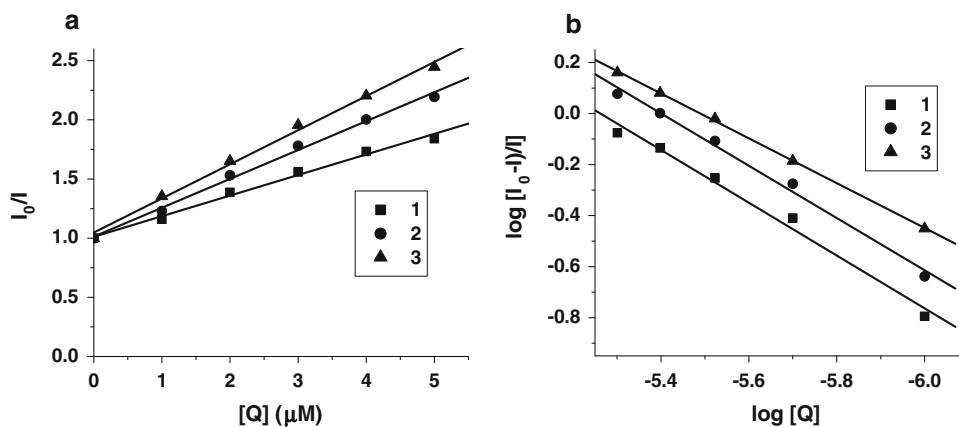


Table 4 Quenching constant (K_q), binding constant (K_{bin}), and number of binding sites (n) for the interactions of compounds with bovine serum albumin

| Compound | K_q (M^{-1}) | K_{bin} (M^{-1}) | n |
|----------|-------------------------------|-------------------------------|------|
| 1 | $1.74 (\pm 0.12) \times 10^5$ | $6.71 (\pm 0.25) \times 10^4$ | 0.88 |
| 2 | $2.44 (\pm 0.09) \times 10^5$ | $2.82 (\pm 0.11) \times 10^5$ | 1.02 |
| 3 | $2.88 (\pm 0.15) \times 10^5$ | $3.45 (\pm 0.08) \times 10^5$ | 1.03 |

indicated that these compounds can be stored and released by the protein.

To further establish the point of interaction of BSA and the compounds, synchronous fluorescence experiments were conducted; these would provide information on the molecular microenvironment, particularly near the fluorophore functional groups [54]. The fluorescence of BSA is due to the presence of tyrosine and tryptophan residues. Of them, tryptophan is the most dominant fluorophore, located at the substrate binding sites. Most of the compounds bind to the protein in the active binding sites. Hence, the synchronous method is usually applied to find out the conformational changes around the tryptophan and tyrosine region. In synchronous fluorescence spectroscopy, according to Miller [55], the difference between the excitation wavelength and the emission wavelength ($\Delta\lambda = \lambda_{em} - \lambda_{ex}$) indicates the type of chromophores. A higher $\Delta\lambda$ value, such as 60 nm, is indicative of the characteristic of a tryptophan residue, whereas a lower $\Delta\lambda$ value, such as 15 nm, is characteristic of a tyrosine residue [56]. The synchronous fluorescence spectra of BSA with various concentrations of the compounds were recorded at $\Delta\lambda = 15$ nm (Fig. 9) and $\Delta\lambda = 60$ nm (Fig. 10). The fluorescence intensity of tyrosine is very slightly decreased, but the fluorescence intensity of tryptophan is decreased drastically with increasing concentration of the compounds. This suggested that the interaction of the compounds with BSA protein affects the

conformation of the tryptophan microregion. It further revealed that the hydrophobicity around tryptophan residues is strengthened. The hydrophobicity observed in fluorescence and synchronous measurements confirmed the effective binding of the compounds with the BSA protein. Hence, the strong interaction of these compounds with BSA protein suggested that the compounds are potential candidates for further biological studies such as antioxidative and anti-cancer studies.

Evaluation of radical scavenging ability

Since the experiments reported so far revealed that the ligand and its copper(II) complexes exhibit good DNA and protein binding affinity, it was considered worthwhile to study the antioxidant activity of these compounds. The antioxidant properties of quinoline derivatives have attracted a lot of interest and have been extensively investigated, mainly in *in vitro* systems [57, 58]. The radical scavenging activities of our compounds along with the standards butylated hydroxyanisole and butylated hydroxytoluene in a cell-free system were examined with reference to hydroxyl radicals, DPPH radicals, nitric oxide, superoxide anion radicals, and the determination of IC_{50} values. No significant radical scavenging activities were observed in all the experiments performed with $CuCl_2$ and $Cu(NO_3)_2$, even up to 1.0 mM concentration under the same experimental conditions. The IC_{50} values (Table 5) indicated that the three compounds showed antioxidant activity in the order $3 > 2 > 1$ in all the experiments. The superoxide anion radical scavenging power of the compounds tested was the greatest and the nitric oxide scavenging power was the least.

These results are much better than the result observed for standard antioxidants, butylated hydroxyanisole and butylated hydroxytoluene, except in the DPPH radical

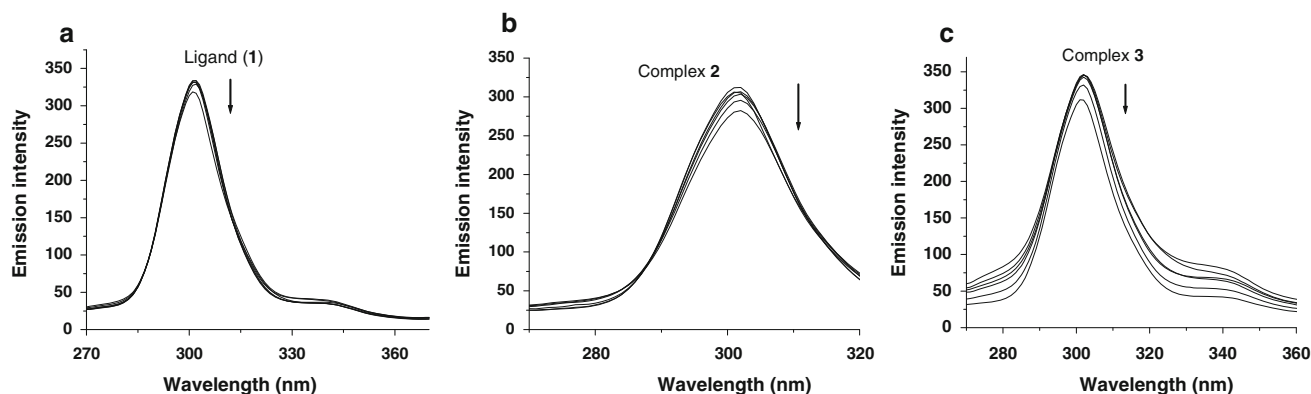


Fig. 9 Synchronous spectra of BSA (1 μM) in the presence of increasing amounts of compounds **1** (a), **2** (b), and **3** (c) (0, 1, 2, 3, 4, and 5 μM) for a wavelength difference of $\Delta\lambda = 15$ nm. Arrows show the emission intensity decrease upon increasing the concentration of the compounds

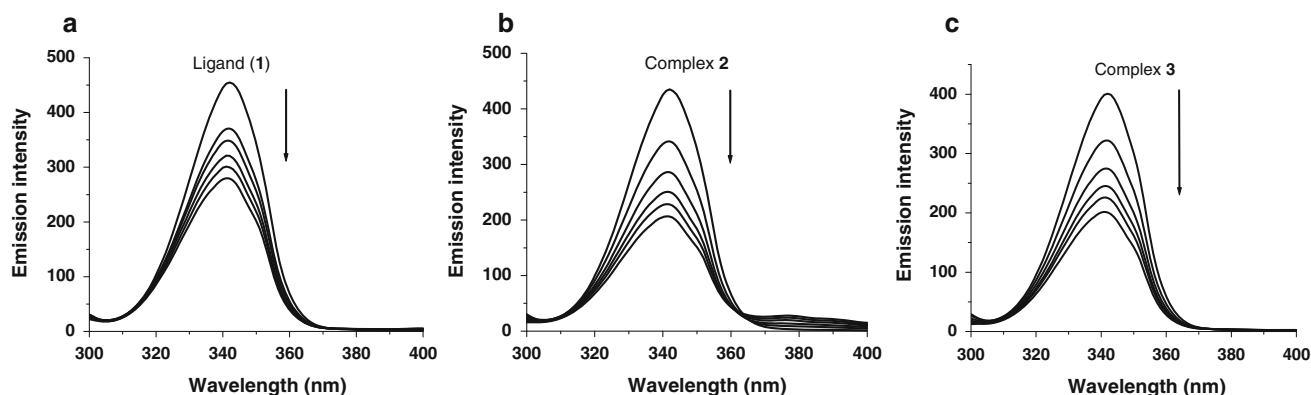


Fig. 10 Synchronous spectra of BSA (1 μM) in the presence of increasing amounts of compounds **1** (a), **2** (b), and **3** (c) (0, 1, 2, 3, 4 and 5 μM), for a wavelength difference of $\Delta\lambda = 60$ nm. Arrows show the emission intensity decrease upon increasing the concentration of the compounds

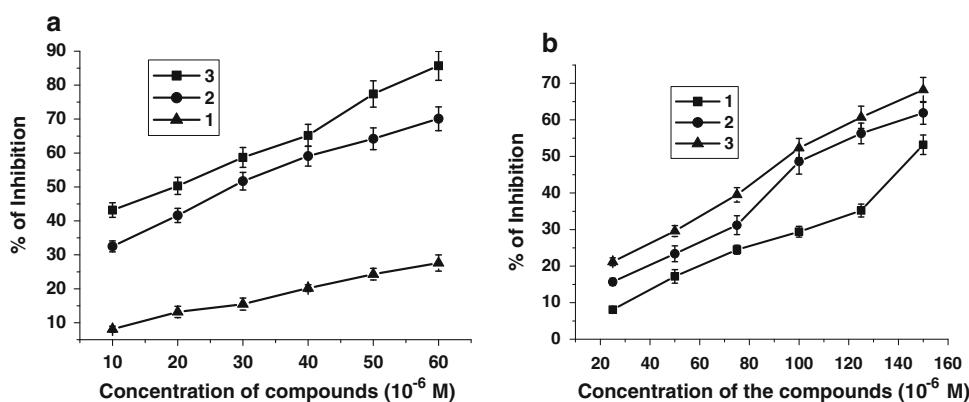
Table 5 IC_{50} values (μM) calculated from various radical scavenging assays of compounds **1**, **2**, and **3** and the standards butylated hydroxyanisole (BHA) and butylated hydroxytoluene (BHT)

| Compound | $\text{OH}\cdot$ | NO | DPPH \cdot | $\text{O}_2^{\cdot-}$ |
|----------|------------------|----------------|------------------|-----------------------|
| 1 | 128 ± 6 | 181 ± 5 | 161 ± 4 | 91.3 ± 4.5 |
| 2 | 17.2 ± 1.5 | 68.6 ± 4.3 | 33.1 ± 2.2 | 8.16 ± 1.24 |
| 3 | 9.18 ± 0.93 | 27.4 ± 2.3 | 18.92 ± 1.40 | 3.12 ± 0.53 |
| BHA | 312 ± 6 | 621 ± 11 | 9.79 ± 0.92 | 297 ± 8 |
| BHT | 278 ± 8 | 726 ± 8 | 9.87 ± 0.75 | 278 ± 5 |

DPPH 2,2'-diphenyl-1-picrylhydrazyl

assay. From the results obtained for the two copper(II) complexes, it can be inferred that the difference in the planarity of the structures and counterions present in the complexes is likely to induce variations in antioxidant activities. The enhanced planarity of the complexes over the free ligand is the reason for the enhanced antioxidant activity of the two copper(II) complexes over the ligand. Among the two complexes, the highest activity for **3** is due to the greater planarity of the square-planar geometry compared with the square-pyramidal geometry of **2**.

Fig. 11 Cytotoxic activity of compounds **1**, **2**, and **3** against HeLa (a) and HEP-2 (b) cells



Cytotoxic activity evaluation by MTT assay

The positive results obtained from DNA binding, BSA binding, and antioxidation studies of **1**, **2**, and **3** encouraged us to test their cytotoxicity against some cancer cells. The results of cytotoxicity assays of the activity of the ligand and the copper(II) complexes against the human cervical cancer cell line (HeLa) and human laryngeal epithelial carcinoma cells (HEp-2) are shown in Fig. 11. The biological assays of the ligand and the copper(II) complexes show that the copper(II) complexes exhibit greater activities than the corresponding ligand against HeLa and HEp-2 cells. The IC_{50} value of **3** demonstrated a much higher inhibitory effect than for **2** and **1** (Table 6).

The compounds are more active on HeLa cells than on HEp-2 cells. The cytotoxic activity studies in vitro indicate that the two copper(II) complexes have better activities than the corresponding ligand but showed significantly less activity than cisplatin. In addition, the IC_{50} values of all the compounds for NIH 3T3 mouse embryonic fibroblasts (normal cells) were above 300 μM , which confirmed that the compounds act very specifically on cancer cells. But, copper(II) chloride and copper(II) nitrate did not show any

Table 6 IC₅₀ values (μM) of compounds **1**, **2**, and **3** and cisplatin for activity against HeLa and HEP-2 cancer cells

| Compound | HeLa | HEP-2 |
|-----------|-------------|-------------|
| 1 | 127 ± 5 | 145 ± 4 |
| 2 | 28.3 ± 1.6 | 105 ± 3 |
| 3 | 19.3 ± 1.2 | 95.4 ± 2.1 |
| Cisplatin | 3.73 ± 0.17 | 2.32 ± 0.24 |

significant activity on the cancer cells even up to 500 μM concentration, which confirmed that the copper(II) chelation with the ligand is the only factor responsible for the observed cytotoxic properties of the new complexes. The better cytotoxic activities of the two copper(II) complexes in comparison with the ligand may be attributed to the extended planar structure induced by the $\pi \rightarrow \pi^*$ conjugation resulting from the chelating of the metal ion with the ligand. In addition, the inhibitory rate of **3** against HeLa and HEP-2 cancer cells is higher than that of **2** (Fig. 11), which may be due to the square planarity and the presence of a nitrate coligand in **3**. These findings of cytotoxic activities in vitro are further evidence to show that the complexes and the free ligand bind to DNA, leading to cell death.

Conclusion

Novel 2-oxo-1,2-dihydroquinoline-3-carbaldehyde (4'-methylbenzoyl) hydrazone (H₂L) (**1**) and its two copper(II) complexes have been synthesized. Single-crystal X-ray diffraction studies revealed that the structure of [Cu(H₂L)Cl₂] \cdot 2H₂O (**2**) is square pyramidal and that of [Cu(HL)NO₃] \cdot DMF (**3**) is square planar. The change of counterion (Cl⁻ to NO₃⁻) in the copper(II) salts altered the coordination mode of hydrazone from ONO to ONO⁻ and the geometry from square pyramidal to square planar in the resulting complexes. The DNA binding properties of the two copper(II) complexes and the free ligand were investigated by absorption and fluorescence measurements. The results supported the fact that the compounds bind to CT-DNA via intercalation. The binding constants show that the DNA binding affinity increased in the order **1** < **2** < **3**. The protein binding properties of the compounds examined by the fluorescence spectra suggested that the binding affinity of the square-planar complex (**3**) for BSA is stronger than that of the square-pyramidal complex (**2**) and the ligand. In addition, the compounds also exhibited good antioxidant activities, and the activity of **3** is better than that of **2** and **1**. All three compounds showed considerable cytotoxic activity against HeLa and HEP-2, and the values indicated that the cytotoxic activity of **3** is greater than that of **2** or the free ligand (**1**). So, overall, a structure-dependent biological

activity was observed and was well explained on the basis of structural planarity. The findings are significant for us to explore further the DNA and protein interaction and anti-oxidative and cytotoxic activities of the transition metal complexes containing different 2-oxo-1,2-dihydroquinoline-3-carbaldehyde Schiff bases.

Acknowledgments Financial assistance received from the Council of Scientific and Industrial Research, New Delhi, India [grants 01(2216)/08/EMR-II and 21(0745)/09/EMR-II], is gratefully acknowledged. We would also like to thank G. Paramaguru and R. Ranganathan (School of Chemistry, Bharathidasan University, India) for their help in experimental work regarding EB–DNA displacement.

References

- Friedman AE, Kumar CV, Turro NJ, Barton JK (1991) *Nucleic Acids Res* 19:2595–2602
- Pyle AM, Morii T, Barton JK (1990) *J Am Chem Soc* 112:9432–9434
- Pizarro AM, Sadler PJ (2009) *Biochimie* 91:1198–1211
- Raja NS, Nair BU (2008) *Toxicology* 251:61–65
- Burrows CJ, Rokita SE (1994) *Acc Chem Res* 27:295–301
- Banerjee AR, Jaeger A, Turner DH (1993) *Biochemistry* 32:153–163
- Tanaka T, Yukawa K, Umesaki N (2005) *Oncol Rep* 14:1365–1369
- Wang D, Lippard SJ (2005) *Nat Rev Drug Discovery* 4:307–320
- Berners-Price SJ, Appleton TG (2000) *Platinum-based drugs in cancer therapy*. Humana Press, Totowa
- Angeles-Boza AM, Bradley PM, Fu PKL, Wicke SE, Bacsa J, Dunbar KM, Turro C (2004) *Inorg Chem* 43:8510–8519
- Kumar CV, Barton JK, Turro NJ (1985) *J Am Chem Soc* 107:5518–5523
- Xu H, Zheng KC, Chen Y, Li YZ, Lin LJ, Li H, Zhang PX, Ji LN (2003) *Dalton Trans* (11):2260–2268
- Mahadvan S, Palaniandavar M (1997) *Inorg Chim Acta* 254:291–302
- Xu H, Zheng KC, Deng H, Lin LJ, Zhang QL, Ji LN (2003) *New J Chem* 27:1255–1263
- Asadi M, Safaei E, Ranjbar B, Hasani L (2004) *New J Chem* 28:1227–1234
- Chaires JB (1998) *Biopolymers* 44:201–215
- Sadhukhan D, Ray A, Das S, Rizzoli C, Rosair GM, Mitra S (2010) *J Mol Struct* 975:265–273
- Silveira VC, Luz JS, Oliveira CC, Graziani I, Ciriolo MR, Ferreira AMC (2008) *J Inorg Biochem* 102:1090–1103
- Zhang S, Zhu Y, Tu C, Wei H, Yang Z, Lin L, Ding J, Zhang J, Guo Z (2004) *J Inorg Biochem* 98:2099–2106
- Garcia-Gimenez JL, Gonzalez-Alvarez M, Liu-Gonzalez M, Macias B, Borrás J, Alzuet G (2009) *J Inorg Biochem* 103:923–934
- Aplegot S, Coppey J, Fromentin A, Guille E, Poupon MF, Roussel A (1986) *Anticancer Res* 6:159–165
- Atkinson A, Winge DR (2009) *Chem Rev* 109:4708–4721
- Tseng CH, Tzeng CC, Yang CL, Lu PJ, Chen HL, Li HY, Chuang YC, Yang CN, Chen YL (2010) *J Med Chem* 53:6164–6179
- DeRuiter J, Brubaker AN, Whitmer WL, Stein JL (1986) *J Med Chem* 29:2024–2028
- Hewawasam P, Fan W, Knipe J, Moon SL, Boissard CG, Gribkoff VK, Starett JE (2002) *Bioorg Med Chem Lett* 12:1779–1783

26. Rousell J, Haddad EB, Mak JC, Webb BL, Giembycz MA, Barnes PJ (1996) *Mol Pharmacol* 49:629–635
27. Ukrainets IV, Gorokhova VO, Benzuglyi AP, Sidorenko VL (2002) *Farm Zh* 1:75–80
28. Krishnamoorthy P, Sathyadevi P, Cowley AH, Butorac RR, Dharmaraj N (2011) *Eur J Med Chem* 46:3376–3387
29. Fan CD, Su H, Zhao J, Zhao BX, Zhang SL, Miao JY (2010) *Eur J Med Chem* 45:1438–1446
30. Zhang Y, Zhang L, Liu L, Guo J, Wu D, Xu G, Wang X, Jia D (2010) *Inorg Chim Acta* 363:289–293
31. Rodriguez-Arguelles MC, Ferrari MB, Bisceglie F, Pelizzi C, Pelosi G, Pinelli S, Sassi M (2004) *J Inorg Biochem* 98:313–321
32. Raja DS, Paramaguru G, Bhuvanesh NSP, Reibenspies JH, Renganathan R, Natarajan K (2011) *Dalton Trans* 40:4548–4559
33. Singh MK, Chandra A, Singh B, Singh RM (2007) *Tetrahedron Lett* 48:5987–5990
34. Bruker AXS APEX2. Program for data collection on area detectors. Bruker AXS, Madison
35. Sheldrick GM (2008) SADABS (version 2008/1). Program for absorption correction for data from area detector frames. University of Göttingen
36. Blois MS (1958) *Nature* 29:1199–1200
37. Nash T (1953) *Biochem J* 55:416–421
38. Green LC, Wagner DA, Glogowski J, Skipper PL, Wishnok JS, Tannenbaum SR (1982) *Anal Biochem* 126:131–138
39. Beauchamp C, Fridovich I (1971) *Anal Biochem* 44:276–287
40. Blagosklonny M, El-diery WS (1996) *Int J Cancer* 67:386–392
41. Liu ZC, Wang BD, Yang ZY, Li Y, Qin DD, Li TR (2009) *Eur J Med Chem* 44:4477–4484
42. Liu ZC, Wang BD, Li B, Yang ZY, Li TR, Li Y (2010) *Eur J Med Chem* 45:5353–5361
43. Hecht SM (2000) *J Nat Prod* 63:158–168
44. Eriksson M, Leijon M, Hiort C, Norden B, Graeslund A (1994) *Biochemistry* 33:5031–5040
45. Nohara A, Umetani T, Sanno Y (1973) *Tetrahedron Lett* 22:1995–1998
46. Meyer-Almes FJ, Porschke D (1993) *Biochemistry* 32:4246–4253
47. Howe GM, Wu KC, Bauer WR (1976) *Biochemistry* 19:339–347
48. Zeng YB, Yang N, Liu WS, Tang N (2003) *J Inorg Biochem* 97:258–264
49. Wang BD, Yang ZY, Wang Q, Cai TK, Crewdson P (2006) *Bioorg Med Chem* 14:1880–1888
50. Raja DS, Bhuvanesh NSP, Natarajan K (2011) *Eur J Med Chem* 46:4584–4594
51. Chakraborty B, Basu S (2009) *J Lumin* 129:34–39
52. Han XL, Mei P, Liu Y, Xiao Q, Jiang FL, Li R (2009) *Spectrochim Acta A* 74:81–787
53. Skyrianou KC, Perdih F, Turel I, Kessissoglou DP, Psomas G (2010) *J Inorg Biochem* 104:740–749
54. Chen GZ, Huang XZ, Xu JG, Wang ZB, Zhang ZZ (1990) *Method of fluorescent analysis*, 2nd edn. Science Press, Beijing
55. Miller JN (1979) *Proc Anal Div Chem Soc* 16:203–208
56. Brustein EA, Vedenkina NS, Irkova MN (1973) *Photochem Photobiol* 18:263–279
57. Sankaran M, Kumarasamy C, Chokkalingam U, Mohan PS (2010) *Bioorg Med Chem Lett* 20:7147–7151
58. Malakyan MG, Badzhinyan SA, Vardevanyan LA, Grigoryan DS, Egiazaryan DE, Avetisyan AA, Aleksanyan IL, Ambartsumyan LP, Sargsyan KS (2009) *Pharm Chem J* 43:8–11